

Nanoscale

Accepted Manuscript



This is an *Accepted Manuscript*, which has been through the Royal Society of Chemistry peer review process and has been accepted for publication.

Accepted Manuscripts are published online shortly after acceptance, before technical editing, formatting and proof reading. Using this free service, authors can make their results available to the community, in citable form, before we publish the edited article. We will replace this *Accepted Manuscript* with the edited and formatted *Advance Article* as soon as it is available.

You can find more information about *Accepted Manuscripts* in the [Information for Authors](#).

Please note that technical editing may introduce minor changes to the text and/or graphics, which may alter content. The journal's standard [Terms & Conditions](#) and the [Ethical guidelines](#) still apply. In no event shall the Royal Society of Chemistry be held responsible for any errors or omissions in this *Accepted Manuscript* or any consequences arising from the use of any information it contains.

Erythrocyte Membrane-Coated Biomimetic Nanovectors with Programmed Delivery and Near-Infrared Light Triggering Properties for Photodynamic Therapy of Cancer

Hui Ding,^a Yanlin Lv,^a Dezhi Ni,^b Jie Wang,^a Zhiyuan Tian,^{a*} Wei Wei,^{b*} Guanghui Ma^{b*}

^a School of Chemistry and Chemical Engineering, University of Chinese Academy of Sciences, Beijing 100049, P. R. China,

^b National Key Laboratory of Biochemical Engineering, Institute of Process Engineering, CAS Beijing 100190, P. R. China,

E-mail: zytian@ucas.ac.cn; weiwei@ipe.ac.cn; ghma@ipe.ac.cn

Keywords: photodynamic therapy, erythrocyte membrane, programmed delivery, cancer, singlet oxygen

Abstract: A new type of photodynamic therapy (PDT) agents using the upconversion nanoparticles (UCNPs) with incorporated photosensitizers as the inner core and erythrocyte membrane (RM) decorated with dual targeting moieties as cloak is developed. Owing to the endogenous nature of RM, the RM-coating endows the PDT agents with perfect biocompatibility and stealth ability to escape from the entrapment of reticulo-endothelial system (RES). More importantly, owing to the unique nature of erythrocyte as oxygen carrier in blood, the RM outer layer of the agents unequivocally facilitates the permeation of ground-state molecular oxygen ($^3\text{O}_2$) and the singlet oxygen ($^1\text{O}_2$) as compared to the previously developed PDT agents with other types of coating. Another salient feature of the as-prepared PDT platform is the decoration of RM with dual targeting moieties for selective recognition of cancer cells and mitochondria targeting, respectively. The synergistic effect of RM coating and dual-targeting of such feature-packed agents is investigated in tumor-bearing mice

and the improved PDT therapeutic efficacy is confirmed, which is the first paradigm where RM-coated NIR-triggered nanovectors with programmed delivery ability applied in PDT of tumor *in vivo*.

1. Introduction

Photodynamic therapy (PDT) has emerged as a clinical treatment modality for a variety of diseases including cancers.¹⁻³ The cornerstone of PDT is light-triggered photosensitizer (PS)-mediated conversion of ground-state molecular oxygen ($^3\text{O}_2$) to singlet oxygen ($^1\text{O}_2$), a highly reactive species capable of killing cancer cells, destroying the tumor vasculature, and activating a non-specific immune response.⁴⁻¹² The practical PDT therapeutic efficacy critically relies on the precision delivery of PS to the target lesions and efficient generation and release of $^1\text{O}_2$ and the PDT agents play crucial role in achieving such goal. A variety of efforts have been devoted to optimizing the properties of PDT agents via either endowing PDT agents with recognition function and/or enhancing the yield of $^1\text{O}_2$. Many nanoparticle (NP)-based systems have been developed as carriers for delivering PS to the pathological sites via the way of passive or active targeting.¹³⁻¹⁷ Specifically, nanoconstructs with outer encapsulation of silica, titania, polymer, chitosan, ferritin were developed as PS carriers; and the improved solubility in aqueous milieu, biocompatibility, stability of these carriers upon coating were confirmed.¹⁸⁻²⁶ To minimize the photodamage to the “normal” cells originating from the undesired interactions between the PDT agents and the non-targeted cells or tissues,²⁷ biomolecular recognition moieties such as

peptide, protein conjugates, folic acid, and aptamers were used to endow PDT agents with high selectivity and ability of precision localization at the target lesions.²⁸⁻³¹

The conventional PDT uses photosensitizers that are usually triggered via visible light and therefore suffer from the limited penetration depth of the activation light in the cases of treating deep-seated disease cells or cancerous issues. As a strategy to circumvent such impediment of limited penetration depth of the visible activation light, the upconversion nanoparticles (UCNPs)³²⁻³⁶ capable of converting NIR photon into visible photon were employed as the light transducer to activate the PS and enable NIR-triggered PDT treatment, via Förster resonance energy transfer (FRET) from UCNPs to PS. Moreover, a powerful strategy with the involvement of single-wavelength excitation of UCPNs and FRET from UCNPs to two types of PS, with the aim of increasing the yield of $^1\text{O}_2$, was developed and the enhanced PDT therapeutic efficacy was confirmed.¹⁸

In spite of considerable amount of efforts devoted, the exploitation of PDT agents with optimized properties in terms of each aspect still remains the ultimate challenge. Specifically, NP-based agents during delivering are usually opsonized and cleared by the spleen, liver and other parts of the reticulo-endothelial system (RES), which results in short blood circulation time and limited opportunities of PDT agents to reach the tumor site via the EPR (enhance permeation and retention) effect.^[37,38] In terms of targeting performance of PDT agents, tumor-guiding moieties indeed improve the cellular uptake and increase the intracellular $^1\text{O}_2$ concentration. Such a primary targeting strategy, however, is good at guiding the agents into target cells, but

cannot accomplish highly localized distribution of the agents within the subcellular targets due to the nonspecific intracellular distribution, which will dilute the power of $^1\text{O}_2$ to the subcellular targets.^{28,30} It is also critical in PDT to accumulate $^1\text{O}_2$ with high local concentration at the ultimate sites so as to destroy the vital subcellular targets to a maximum extent, which demands the agents to produce $^1\text{O}_2$ with high efficiency and release $^1\text{O}_2$ from the agents before such short-lived (in microsecond level) species lose its reactivity.³⁹

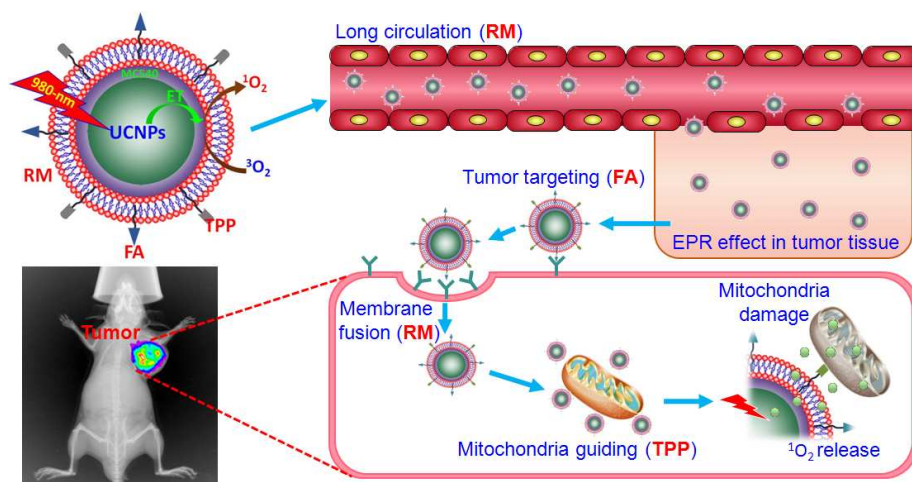


Figure 1. Schematic illustration of UCNPs-based RM-coated dual-targeted biomimetic NPs (not to scale); the long blood-circulation time of NPs enabling their accumulation at the tumor site by EPR effect; and dual-targeted feature of the agents facilitating the uptake of the target cancer and their efficient location at mitochondria.

In this work, we developed UCNPs-based RM-coated biomimetic PDT agents with folate (FA) and triphenylphosphonium (TPP) cation decorated on the surface for in vivo PDT treatment of tumors (**Figure 1**). Such type of feature-packed PDT agents was constructed by incorporating the PS MC540 in the shell around the UCNPs and the following encapsulation of the resulting photoactive cores, denoted as Us/PS, with a RM layer via a strategy of mechanical extrusion.⁴⁰ Two targeting moieties,

DSPE-PEG₂₀₀₀-FA and DSPE-PEG₂₀₀₀-TPP (DSPE-PEG₂₀₀₀, 1,2-distearoyl-sn-glycero-3-phosphoethanolamine-N-[methoxy(poly-ethyleneglycol)]) were inserted into the phospholipid layer of RM during the process of extrusion. These agents are capable of generating ¹O₂ upon 980-nm irradiation based on the light transducing ability of UCNPs. Additionally, the RM-coating endows these agents with perfect biocompatibility and stealth ability to escape from the RES as compared to those agents with non-biological coating.⁴⁰⁻⁴³ More importantly, owing to the unique nature of erythrocyte as oxygen carrier in blood, the PDT agents with RM exterior developed in the present work is expected to possess unique and overwhelming advantage in terms of the ability for facilitating the permeation of both ³O₂ and ¹O₂ species as compared to the previously developed PDT agents with other types of coating such as silica, titania, polymer, and even those with biological coating such as chitosan and ferritin. Such an advantage remains nearly unheeded in other types of red blood cell (RBC)-mimicking systems but is crucial in ensuring the efficacy of PDT agents because sufficient supply of oxygen is highly desired for the generation of ¹O₂ with sufficient concentration in PDT treatment. Another salient feature of these PDT agents is the decoration of RM layer with dual targeting moieties for selective recognition of cancer cells and accurate mitochondria guiding.⁴⁴⁻⁴⁶ The synergistic effect of RM coating and FA/TPP dual-targeting of the PDT agents was investigated via in vivo PDT test on tumor-bearing mice and the significantly improved PDT therapeutic efficacy was confirmed, which is the first demonstration of RM-coated

PDT nanovectors with programmed delivery and NIR-triggering ability applied in PDT in vivo.⁴⁷⁻⁴⁹

2. Results and Discussions

The NaYF₄:Yb/Er UCNPs were synthesized according to the literature procedure with minor modifications.⁴² The size and morphology of the nanoparticles were characterized by transmission electronic microscopy (TEM), as shown in **Figure S2**. The UCNPs prepared via this method are not dispersible in aqueous solution owing to the presence of oleic acid (OA) on their surface. Taking this, a typical type of amphiphilic triblock copolymers, Pluronic[®]F-127, was used to modify the surface of UCNPs with the purpose of fulfilling the oil-to-water phase transfer. Amphiphilic F-127 copolymer typically possesses a hydrophobic polypropylene oxide (PPO) segment sandwiched between two hydrophilic polyethylene oxide (PEO) segments. During the phase transfer, the PPO segment was expected to entwine with the OA components around UCNPs via hydrophobic interactions while the PEO segments extended into the aqueous phase. Simultaneously, incorporation of the photosensitizer MC540 was fulfilled during this phase transfer process by entrapping MC540 within the hydrophobic shell consisting of OA and PPO segments owing to hydrophobic interactions. After extrusion processing, these NPs were successfully coated with RM (**Figure S1c**). DSPE-PEG₂₀₀₀-Folate and DSPE-PEG₂₀₀₀-PPh₃ ligand were decorated on the RM surface during the process of extrusion. The evolution in particle size and the zeta potential voted the success of FA and TPP decoration on the surfaces of the agents (Table S1).

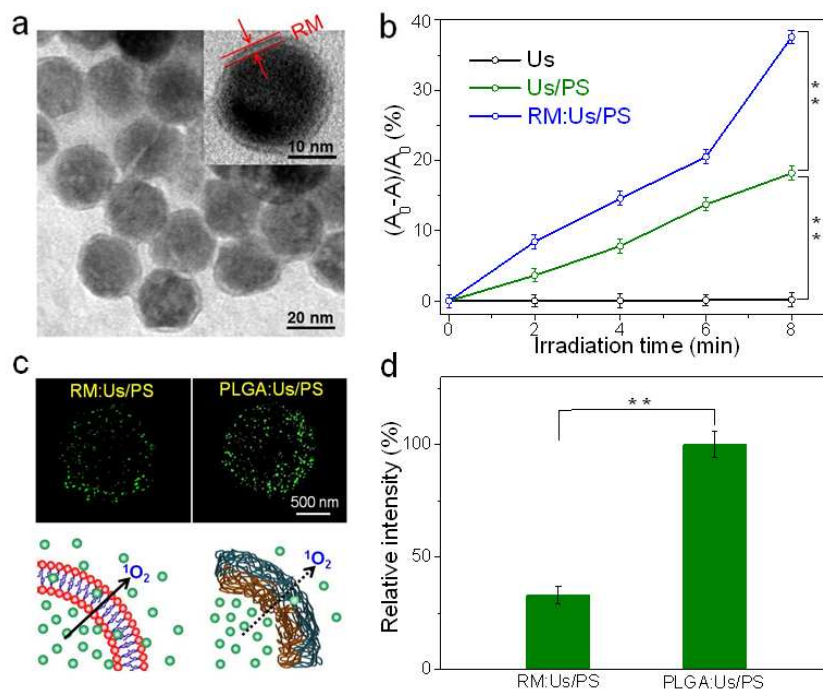


Figure 2. a) The typical TEM image of the F/P-RM:Us/PS. b) The absorbance of ABDA as a function of irradiation (980-nm) time in presence of the pristine UCNP, Us/PS, and RM:Us/PS, respectively. (** $P < 0.01$). c) Comparison of 1O_2 release rate from RM- and PLGA-coated Us/PS. d) Comparison of the residual 1O_2 in RM- and PLGA-coated Us/PS determined by the fluorescent 1O_2 probe. (** $P < 0.01$).

TEM characterization of these PDT agents, denoted as F/P-RM:Us/PS, displayed their spherical shape with cloaked RM layer, as shown in **Figure 2a**, while dynamic light scattering (DLS) measurement of the same batch of sample reported an average hydrodynamic radius of ~ 45 nm and a narrow polydispersity less than 0.1 (**Figure S3**). Their particle size and zeta potential were well maintained in cell culture media (**Figure S4a** and b), and no aggregation was found during two weeks (Figure S4c). Such a good colloid stability could fulfill the requirements for intravenous injection. The ability of 1O_2 generation of the PDT agents upon NIR light triggering was verified using a water-soluble 1O_2 sensor, 9, 10-anthracenediyl-bis (methylene) dimalonic acid (ABDA), which typically displays 1O_2 -sensitive changes in its

absorption and fluorescence emission features. The pristine UCNPs upon 8-min irradiation of 980-nm light did not lead to discernable change in the absorbance of ABDA, suggesting no generation of $^1\text{O}_2$ (Figure 2b). In contrast, Us/PS resulted in destruction of 18% ABDA under the identical condition, indicating the effectiveness of $^1\text{O}_2$ generation. As expected, destruction of ABDA up to 37.6% was obtained in the case of RM:Us/PS, unequivocally verifying the unique advantage of RM coating for efficient $^1\text{O}_2$ generation. No noticeable leaching or loss of the photosensitizer MC540 was observed, as the ability for destructing ABDA of the agents stored several days was found similar to that of the freshly prepared agents. Taking that $^1\text{O}_2$ has a short half-life, it is highly desired in PDT that $^1\text{O}_2$ interacts with the target structures before it decays and loses reactivity.¹⁸ Thus, the prompt release of $^1\text{O}_2$ from the PDT agents following its generation is a crucial step for an effective PDT outcome. Owing to the unique nature of erythrocyte as oxygen carrier, RM is expected to facilitate the two-way oxygen permeation as compared to other non-biological materials, *i.e.* the ground-state molecular oxygen ($^3\text{O}_2$) flowing through the RM and entering into the inner core of agents for production of $^1\text{O}_2$ and then releasing the latter from the agents. To testify such speculation, NPs of RM- and PLGA-coated Us/PS with relatively large size were prepared and their $^1\text{O}_2$ releasing performance was evaluated (Figure 2c and 2d). Specifically, the relative amount of residual $^1\text{O}_2$ in the inner core of RM-coated Us/PS was about one third of that in the case of PLGA-coated Us/PS, indicating the overwhelming advantage of the former in the rate and efficacy of $^1\text{O}_2$ release.

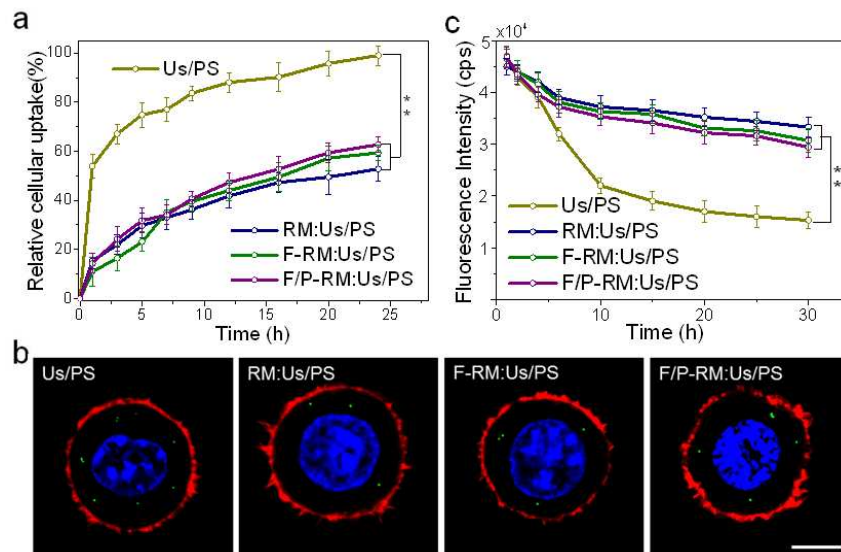


Figure 3. a) Internalization kinetics of different types of NPs in J774A.1 cells. b) The CLSM images of the J774A.1 cells with internalized NPs. c) Evolution of fluorescence intensity of dye-labeled NPs with different formulation in mouse blood.

The longer blood circulation time can offer agents more opportunities to reach the tumor site via the EPR effect. To verify the stealth effects of RM-based biomimetic strategy, the macrophage uptake of agents with different formulation was comparatively evaluated. As shown in **Figure 3a** and b, a small number of Us/PSs were internalized into macrophage due to the hydrophilic outer layer of Us/PS. In contrast, once the Us/PS was coated with RM, the number of internalized NPs obviously decreased, suggesting the perfect stealth ability that the RM coating enabled. Further FA and TPP decorations only showed a very tiny compromise on the stealth effect of cloaked RM. An additional *in vivo* verification experiment was performed by intravenously injecting mice with different types of agents and then monitoring the time-elapsed change in concentration of the dye-labeled agents in the blood (Figure 3c). As expected, the cloaked RM bestowed Us/PS much longer circulating time, since this strategy could disguise our agents as “self” in the blood

stream. Specifically, ~32% of the initial pristine Us/PS left in the blood stream after 30-h circulating. In contrast, ~74% of the initial RM-Us/PS survived under the identical condition, 2.3 times of the counterpart value in the case of pristine Us/PS. Beyond doubted, such biomimetic strategy bestowed remarkably improved stealth ability on the PDT agents, which is expected to play crucial role in determining the ultimate PDT treatment efficacy.^{50,51}

For PDT agents, their high binding affinity with cancer cells is undoubtedly crucial for efficient accumulation in the tumor site and optimized therapeutic outcome. Taking this, we evaluated the effect of ligand decoration on the binding affinity of the agents to B16 cancer cell. As shown in **Figure 4a** and 4b, only a few pristine Us/PS were internalized into cells after 24-h incubation and RM cloaking did not markedly arouse the appetite of the cells. In contrast, the cells displayed markedly promoted uptake of RM:Us/PS with FA targeting owing to the preferential binding of FA to the FA receptor that was highly expressed on the surfaces of cells. Upon further decoration of TPP, an additional increase, ~28%, in the number of internalized agents was observed, likely a result of the electrostatic interaction between positive charged TPP and the cell membrane. The typical CLSM images of cells with internalized NPs clearly demonstrated such uptake discrepancy due to the distinct surface properties of the NPs (Figure 4b), which attributed to the great disparity in intracellular $^1\text{O}_2$ production upon NIR irradiation (Figure 4c and 4d). As compared to the faint fluorescence signal in Us/PS group and the slightly increased brightness in RM:Us/PS group, the markedly promoted internalization of the agents in the FA modification

groups enabled intracellular $^1\text{O}_2$ with much higher concentration shedding light on subsequent PDT. Specifically, the detected intracellular $^1\text{O}_2$ concentration in F/P-RM:Us/PS group is more than 4 times larger than that in the case of Us/PS group.

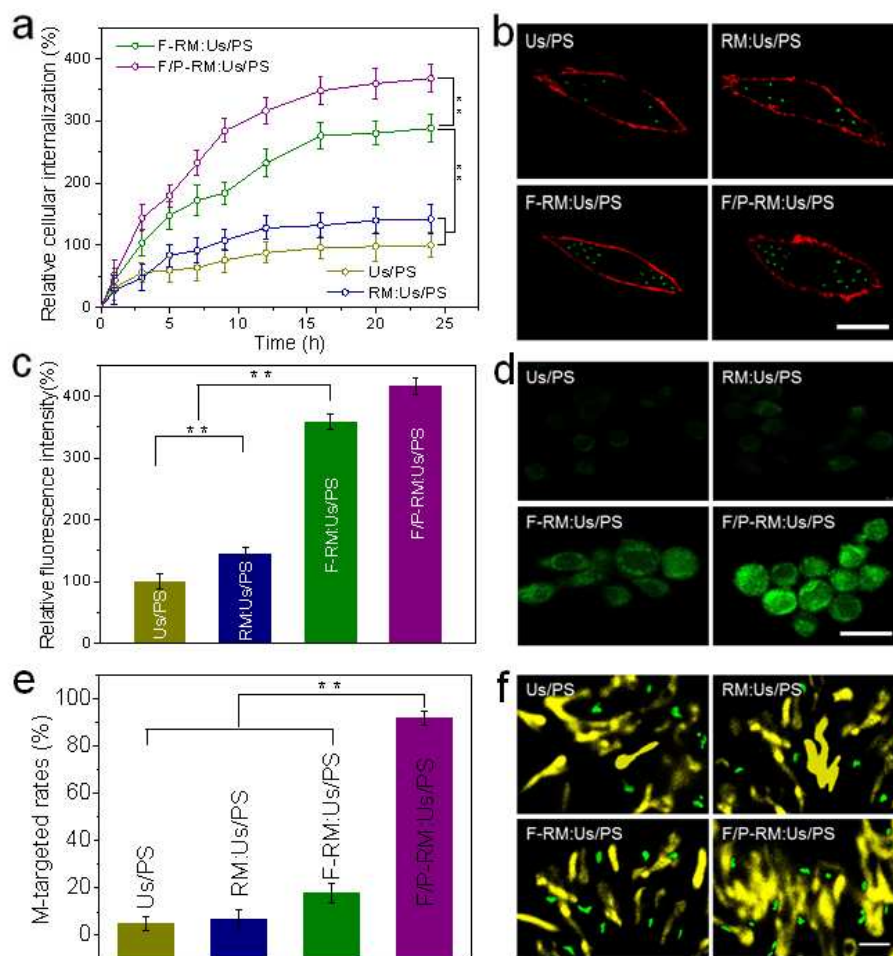


Figure 4. (a, b) Internalization kinetics of different types of NPs in B16 cells and the corresponding CLSM images of cells with internalized NPs (scale bar: 10 μm); (c, d) relative fluorescence intensity and the corresponding CLSM images of B16 cells with internalized $^1\text{O}_2$ probe and different types of NPs (scale bar: 20 μm); (e, f) relative mitochondrion-targeted rate and the corresponding CLSM images of mitochondria (yellow area) with coupled NPs (green dots) (** $P < 0.01$). Scale bar: 500 nm

Mitochondria are vital subcellular organelles and function as the powerhouse of cells. When the mitochondrion is damaged upon exposure to hazardous stimuli like $^1\text{O}_2$, it releases apoptosis inducing factor and triggers the cell death.⁵² In this case,

only the generated ROS components are effectively ferried to mitochondria, can the best PDT performance be achieved. To this end, we investigated the talent of TPP on mitochondria guidance (Figure 4f). The internalized pristine Us/PS were mostly sequestered in lysosomal compartments and few of them (below 5%) could arrive mitochondria area (**Figure S6**). Although RM cloaking could induce membrane fusion process and help the NPs escape from the lysosome (**Figure S7**), the mitochondria targeting rates in RM:Us/PS and F-RM:Us/PS group were still unsatisfactory due to the random intracellular distribution. In sharp contrast, most F/P-RM:Us/PS bound to mitochondria with the targeting rate jumped up to ~92%, confirming the excellent mitochondria guidance of TPP.^{44,45,53,54}

Taking the growing safety concerns about the use of artificial NPs in biological systems, we evaluated the cytotoxicity of the agents themselves. As shown in **Figure 5a**, only little cytotoxicity was found when B16 cells were treated with our agents devoid of 980-nm light irradiation, indicating their good biocompatibility. Specifically, in the case of cells after incubation with F/P-RM:Us/PS with 25 $\mu\text{g/mL}$ UCNPs devoid of 980-nm light irradiation, only ~3.3% decrease in the cell viability was observed. In contrast, all formulations upon exposure to 980-nm light exhibited detectable cytotoxicity (Figure 5b); and the cell viability displayed gradual decrease in sequence of Us/PS, RM:Us/PS, F-RM:Us/PS and F/P-RM:Us/PS in each group with identical UCNPs concentration, indicating the crucial role of RM coating and targeting in the final PDT therapeutic efficacy. Specifically, in the group with 25 $\mu\text{g/mL}$ of UCNPs, only ~20% decrease in the cell viability was observed in the case

of pristine UCNP/PS; and the cell viability further decreased when the UCNP/PS was coated with RM and decorated with targeting moiety FA. Further decoration of RM-coated and FA-targeted UCNP/PS with TPP (F/P-RM:Us/PS) resulted in an overall decrease in the cell viability dramatically up to $\sim 75\%$, owing to the abovementioned versatility in each delivery step (Figure 5b).

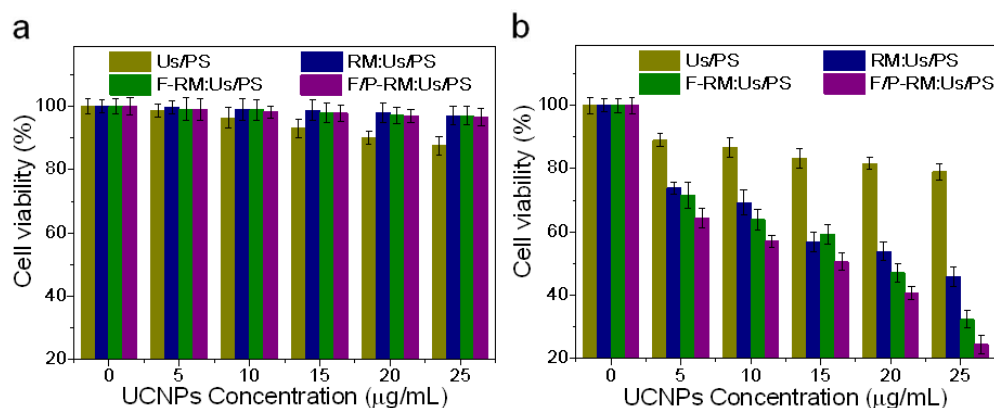


Figure 5. Efficacy of PDT treatment on B16 cells using the model agents with different formulations and incremental concentration devoid of (a) and upon (b) 3-min irradiation of 980-nm light (0.5 W/cm^2).

An effective PDT agent is expected to deliver the PS into tumor tissues so as to maximize the therapeutic outcome while minimizing the side effects. To ascertain this, we partly replaced MC540 with fluorescent Cy7 dye and then evaluated the time-elapsing biodistribution of the agents with different formulations after intravenous injection. As shown in **Figure 6**, no signal of Us/PS at tumor site was detected in the cases with elapsed time less than 48 h and the signal intensity in the case of 48 h was still not satisfactory, indicating the poor affinity of agents to the tumor and most of the agents entrapped in the RES (spleen and liver). Once Us/PS were cloaked with RM, fluorescence signal obtained from the RES 48 h after injection

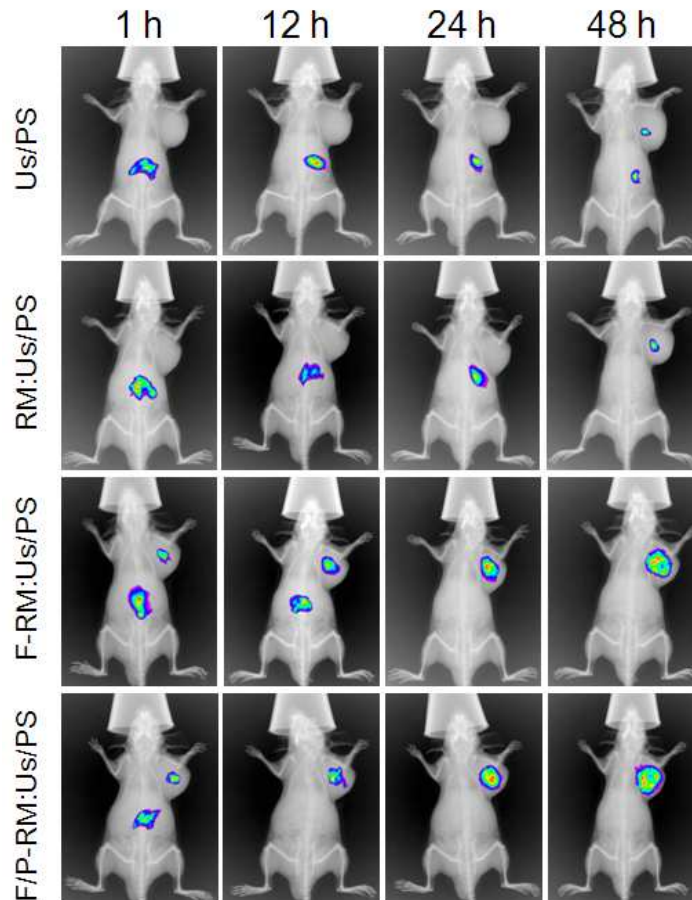


Figure 6. In vivo fluorescence images of real-time tumor targeting characteristics of Us/PS, RM:Us/PS, F-RM:Us/PS, and F/P-RM:Us/PS, respectively, in tumor-bearing mice after intravenous injection.

clearly decreased while signal at tumor site slightly increased, indicating the vital role of RM coating in enabling stealth effects and prolonging the time window for passive accumulation of the agents in tumor tissue. In the F-RM:Us/PS group, fluorescence signal at tumor site was observed only 1 h after the injection and such signal markedly and continuously increased with elapsing time, resulting in a signal 9 times stronger than the counterpart one in the case of pristine Us/PS 48 h after the injection. Unequivocally, such significant improvement confirms the enhanced tumor targeting ability of the agents bestowed by the decoration of FA. Moreover, such excellent

delivery performance could be maintained when F-RM:Us/PS was further functionalized with another targeting moiety TPP. In addition, we also calculated the signal-to-noise (S/N) ratio in the tumor (**Figure S8**). The S/N ratio was very small (<0.3) and little change was observed after the injection of naked Us/PS. In contrast, the ratio in the F/P-RM:Us/PS group constantly increased and reached up to 2.7 at 48 h after injection, further demonstrating the excellent targeted ability.

Inspired by the aforementioned results, we explored the PDT efficacy of the as-prepared model agents *in vivo*. As shown in Figure 7a, all the groups showed tumor inhibition effectiveness as compared with the control group (PBS group). Specifically, the pristine Us/PS exhibited a slight antitumor effect and such efficacy could be meliorated in the case of RM:Us/PS due to the prolonged circulation time, improved efficacy of generation and release of $^1\text{O}_2$. Once FA was decorated on RM, the improved cell uptake resulted in a significant lag in tumor growth. Notably, further decoration with TPP for mitochondria targeting nearly completely stopped the tumor growth via the mechanism of $^1\text{O}_2$ -mediated damage of mitochondria and consuming dissolved oxygen in competition with mitochondria. Specifically, in a quantitative comparison, the tumor volume determined 20 days after PDT treatment using F/P-RM:Us/PS was merely about one tenth of the counterpart value in the case of pristine Us/PS, suggesting a very satisfactory PDT performance of the RM-coated agents with programmed delivery ability. As a result, the survival time of tumor-bearing mice significantly extended upon treatment using F/P-RM:Us/PS, in sharp contrast to that in the Us/PS group (Figure 7b). More detailed information about

nuclear apoptosis in different groups was captured by TUNEL staining of tumor tissue sections (Figure 7c). In agreement with above results, the F/P-RM:Us/PS group induced the greatest cell apoptosis, again comforting the success of our programmed delivery approach for PDT. No obvious toxicities or inflammatory infiltrates were observed in the histological sections of heart, liver, spleen, lung, and kidney (Figure S9), which further confirmed the safety of our PDT agent.

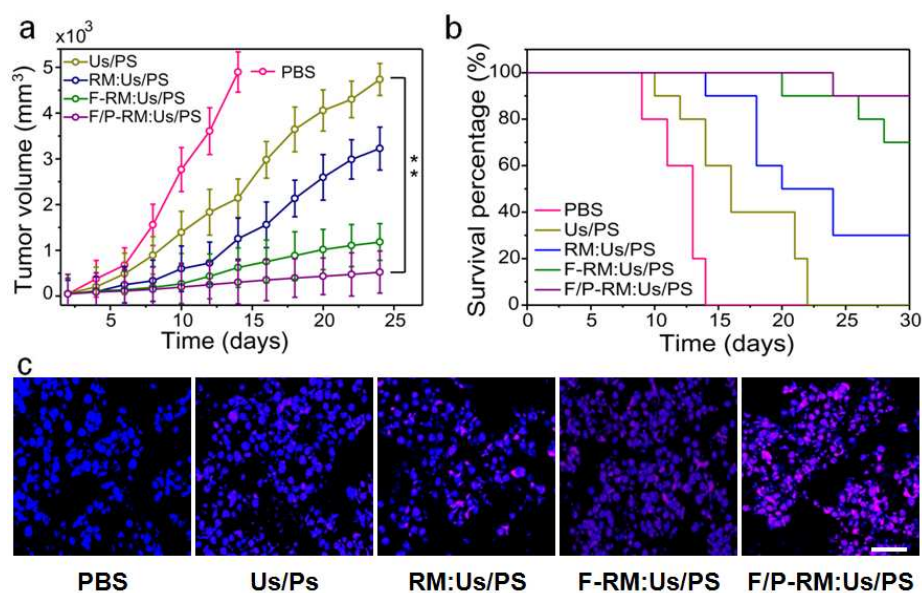


Figure 7. Antitumor efficacies of the model PDT agents with different formulations in B16-bearing mice model. (a) Tumor volumes of mice in PDT treatment groups using different model agents as a function of the number of days after treatment. (b) Survival percentage of mice in different treatment groups. (c) The cell nuclear morphology of tumor tissue. Scale bar: 50 μm.

3. Conclusion

In conclusion, we have developed a novel class of biomimetic PDT nanovectors using UCNPs with incorporated PS as core and RM decorated with dual targeting moieties as cloak for in vivo PDT of tumors. In addition to endowing the nanovectors with superior stealth ability to escape from the RES, the RM-coating significantly

facilitate the ground-state molecular oxygen ($^3\text{O}_2$) entering into the inner core of agents for production of $^1\text{O}_2$ and releasing the latter from the agents as compared to the conventional PDT agents with other types of coating, which was demonstrated to play crucial role in improving the PDT therapeutic outcome. The decoration of RM layer with dual targeting moieties enables selective recognition of cancer cells and accurate mitochondria guiding, respectively. Such feature-packed PDT agents exhibited programmed boost in the delivery performance on blood circulation, tumor accumulation, cellular uptake, mitochondria guiding and $^1\text{O}_2$ transportation. Owing to these advantages, the optimized agents, F/P-RM:Us/PS, almost stop the tumor growth and significantly improved the survival rate of tumor-bearing mice, which is the first paradigm of RM-camouflaged PDT nanovectors with programmed delivery and NIR-activation ability as agent in PDT of tumor in vivo. All these results together voted our F/P-RM:Us/PS as an effective modality for PDT treatment.

4. Experimental details

Reagents and materials: $\text{LnCl}_3 \cdot x\text{H}_2\text{O}$ ($\text{Ln}=\text{Y}$, Yb , Er ; $x \approx 5$, 99.90%), ammonium fluoride (NH_4F , 96%), 1-octadecylen (ODE) and oleic acid (OA) were purchased from Alfa Aesar Reagent Company. PLGA (poly (lactic-co-glycolic acid), lactide: glycolide molar ratio of 75:25, Mw 13 kDa) with end acid group was purchased from Lakeshore (USA). Pluronic[®]F-127, N-hydroxysulfosuccinimide, 1-ethyl-3-(3-dimethylamino-propyl) carbodiimide, 9,10-Anthracenediyl-bis (methylene) dimalonic acid (ABDA), (3-Carboxypropyl) triphenylphosphonium bromide, merocyanine 540 (MC540) were obtained from Sigma Aldrich (USA).

1,2-distearoyl-sn-glycero-3-phosphoethanolamine-N-[methoxy(polyethyleneglycol)](DSPE-PEG) derivatives (DSPE-PEG₂₀₀₀-NH₂ and DSPE-PEG₂₀₀₀-Folate), PC Membranes 0.1 μm and 0.05 μm were purchased from Avanti Polar Lipids (USA). All other reagents were of analytic grade. Roswell Park Memorial Institute (RPMI) 1640 Medium, Fetal bovine serum (FBS), 4, 6-diamidino-2-phenylindole (DAPI), Alex-488-phalloidin, Alex-635-phalloidin, DAPI iodide, and MitoTracker[®] Probes were supplied by Invitrogen (USA). Cell Counting Kit-8 (CCK-8) was bought from Beyotime (China). J774A.1 cells and B16 cells were supplied by American Type Culture Collection (ATCC). Balb/c mice were obtained from the Charles River Laboratories (USA). All animal experiments were performed in compliance with the institutional ethics committee regulations and guidelines on animal welfare.

Synthesis of Us/PS: UCNPs were synthesized following previous literatures.^[42] Amphiphilic triblock copolymer Pluronic[®]F-127 was used to modify the surface of UCNPs via oil-to-water phase transfer. Incorporation of MC540 was fulfilled during this phase transfer process by entrapping MC540 within the hydrophobic shell via hydrophobic interactions. In a typical protocol, 30 mg of Pluronic[®]F-127 and 20 mg of MC540 were added into a 25-mL flask containing 20 mg of UCNPs and 5 mL of CHCl₃, and the solution was stirred overnight at room temperature.

Determination of the loading percentage of MC540 in UCNPs: MC540 encapsulated within the RM-coated UCNPs was determined in triplicate by HPLC with UV detection at 227 nm (LC-20AT, Shimadzu). The MC540 loading percentage was calculated according to the following formula:

$$\text{MC540 loading (\%)} = \frac{\text{Mass of MC540 incorporated into nanoparticles}}{\text{Mass of nanoparticles}} \times 100$$

Preparation of F/P-RM:Us/PS: The RM vesicles were prepared following a literature protocol with a slight modification. Whole blood was extracted from female Babl/c mice (6 ~ 8 w) and then purified by centrifugation (800 ×g, 5min, 4°C) to remove the serum. The hemoglobin was removed via the method of hypotonic medium treatment. The collected RBC ghosts were sonicated in a centrifuge tube for 5 min. The resulting vesicles were then extruded serially through 400-nm, 100-nm and 50-nm polycarbonate porous membranes using an Avanti mini extruder (AME). To fuse the RM vesicles with UCNPs/PS, 1 mg of PS@UCNPs NPs was mixed with RM vesicles and then extruded 5 times through a 50-nm membrane. DSPE-PEG₂₀₀₀-Folate/PPh₃ was added into the mixture in the process of extrusion in order to obtain the targeted PDT NPs system. The morphology of UCNPs was observed by TEM (JEOL, Japan). A Zeta SizerNano ZS (Malvern) was used to take DLS measurements for the characterization of particle size and zeta potential.

In vitro cellular uptake of PDT NPs: B16 and J774A.1 cells were seeded at density of 1×10^5 cells/well in 24-well cell plate and incubated for 24 h to allow cell attachment. Then, Cy5-incorporated model PDT agents were added and went through co-incubation. At different time intervals, the cells were harvested and examined by flow cytometry (CyAn ADP, Beckman Coulter). In the CLSM imaging, cells were first seeded on Petri dishes, and the medium was replaced with medium containing model PDT agents with incorporated Cy5. After 24 h incubation, the medium were

removed, and cells were washed with PBS (pH 7.2) followed by fixing with 4% paraformaldehyde and staining with cell membrane dye DiOC₃ (3) iodide. The fluorescence images of cell membrane and PDT agents were captured by CLSM (Ultraview, PerkinElmer) at 500 ~ 560 nm and 650 ~ 700 nm, respectively.

In vivo NIR fluorescence imaging: To establish B16 tumors model, 2×10^6 melanoma cells suspended in serum-free cell medium were injected on the shoulder of each mouse. After two weeks, tumor-bearing mice were injected with the Cy7-incorporated PDT agents for *in vivo* imaging. At different time intervals, the mice were anesthetized and scanned using an *in vivo* imaging system with a 750-nm excitation bandpass filter and a 790-nm emission filter.

PDT study: In the subcutaneous B16 melanoma model, treatments were started when tumor volume was about 200 mm³ and the mice were randomly divided into five groups (n=10). Mice of the five groups were intravenously administered with PBS (100 μL, pH 7.2), model PDT agents (1 mg/kg of PS) once every day. After the administration, the tumor site on each mouse was radiated by the 980-nm NIR laser at the power density of 0.5 W/cm² for 3 min. Tumor sizes were measured with a digital caliper every other day. Relative tumor volume (RTV) was calculated at each measurement time point (where RTV equals the tumor volume at a given time point divided by the tumor volume of initial treatment). Simultaneously, the body weight of each mouse was measured every day. Mice were sacrificed for humane reasons when the tumor exceeded 4500 mm³. The reserved tumor tissues were made into 10 μm

frozen-section and stained with the TUNEL (TdT-mediated dUTP nick end labeling) Apoptosis Detection Kit for apoptosis analysis by CLSM imaging.

Acknowledgements

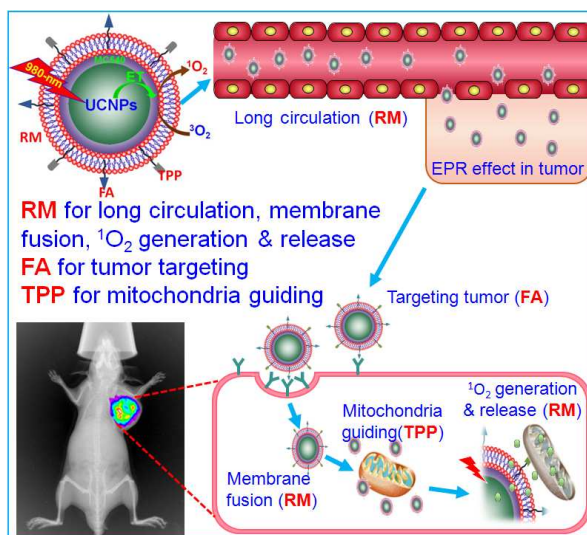
Financial support from the NSFC (No. 21173262 and 21373218), Beijing Nova Program (Z141102001814066), and the “Hundred-Talent Program” of CAS to Z. Y. Tian are acknowledged. Z. Y. Tian thanks Dr. Z. J. Gu, Key Laboratory for Biomedical Effects of Nanomaterials and Nanosafety, CAS, for assistance in synthesis of materials.

Reference

- 1 W. M. Sharman, C. M. Allen, J. E. Van Lier, *Drug Discovery Today* **1999**, 4, 507-517.
- 2 Y. N. Konan, R. Gurny, E. Allemann, *J. Photochem. Photobiol. B*, **2002**, 66, 89-106.
- 3 J. P. Celli, B. Q. Spring, I. Rizvi, C. L. Evans, K. S. Samkoe, S. Verma, B. W. Pogue, T. Hasan, *Chem. Rev.* **2010**, 110, 2795.
- 4 A. M. Fisher, A. L. Murphree, C. J. Gomer, *Lasers Surg. Med.* **1995**, 17, 2-31.
- 5 T. J. Dougherty, C. J. Gomer, B. W. Henderson, G. Jori, D. Kessel, M. Korbelik, J. Moan, Q. Peng, *J. Natl. Cancer Inst.* **1998**, 90, 889-905.
- 6 D. E. Dolmans, D. Fukumura, R. K. Jain, *Nat. Rev. Cancer* **2003**, 3, 380-387.
- 7 A. P. Castano, P. Mroz, M. R. Hamblin, *Nat. Rev. Cancer* **2006**, 6, 535-545.
- 8 P. S. Thong, M. Olivo, K. W. Kho, R. Bhuvaneswari, W. W. Chin, K. W. Ong, K. C. Soo, *J. Environ. Pathol. Toxicol. Oncol.*, **2008**, 27, 35-42.
- 9 J. Wang, G. Z. Zhu, M. X. You, E. Q. Song, M. I. Shukoor, K. J. Zhang, M. B. Altman, Y. Chen, Z. Zhu, C. Z. Huang, W. H. Tan, *ACS Nano* **2012**, 6, 5070-5077.
- 10 J. L. Grimland, C. F. Wu, R. R. Ramoutar, J. L. Brumaghim, J. McNeill, *Nanoscale* **2011**, 3, 1451-1455.
- 11 Y. I. Park, H. M. Kim, J. H. Kim, K. C. Moon, B. Yoo, K. T. Lee, N. Lee, Y. W. Park, D. Ling, *Adv. Mater.* **2012**, 24, 5755-5761.
- 12 M. Wang, Z. Chen, W. Zheng, H. M. Zhu, S. Lu, E. Ma, D. T. Tu, S. Y. Zhou, M. D. Huang, X. Chen, *Nanoscale*, **2014**, 6, 8274-8282.

- 13 D. K. Chatterjee, L. S. Fong, Y. Zhang, *Adv. Drug Delivery Rev.* **2008**, 60, 1627-1637.
- 14 E. Paszko, C. Ehrhardt, M. O. Senge, D. P. Kelleher, J. V. Reynolds, *Photodiagn. Photodyn. Ther.* **2011**, 8, 14-29.
- 15 B. Chen, B. W. Pogue, T. Hasan, *Drug Delivery* **2005**, 2, 477-487.
- 16 L. M. Rossi, P. R. Silva, L. L. Vono, A. U. Fernandes, D. B. Tada, M. S. Baptista, *Langmuir* **2008**, 24, 12534-12538.
- 17 S. J. Lee, H. Koo, H. Jeong, M. S. Huh, Y. Choi, S. Y. Jeong, Y. Byun, K. Choi, K. Kim, I. C. Kwon, *J. Controlled Release*, **2011**, 152, 21-29.
- 18 N. M. Idris, M. K. Gnanasammandhan, J. Zhang, P. C. Ho, R. Mahendran, Y. Zhang, *Nat. Med.*, **2012**, 18, 1580-1585.
- 19 J. N. Shan, S. J. Budijono, G. Hu, N. Yao, Y. Kang, Y. Ju, R. K. Prud'homme, *Adv. Funct. Mater.* **2011**, 21, 2488-2495.
- 20 H. Qian, H. Guo, P. Ho, R. Mahendran, Y. Zhang, *Small*, **2009**, 5, 2285-2290.
- 21 C. Wang, H. Tao, L. Cheng, Z. Liu, *Biomaterials*, **2011**, 32, 6145-6154.
- 22 X. H. Liu, H. S. Qian, Y. P. Ji, Z. Q. Li, Y. Shao, Y. Hu, G. X. Tong, L. C. Li, W. D. Guo, H. C. Guo, *RSC Adv.*, **2012**, 2, 12263-12268.
- 23 M. González-Béjar, M. Liras, L. Francés-Soriano, V. Voliani, V. Herranz-Pérez, M. Duran-Moreno, J. M. García-Verdugo, E. L. Alarcon, J. C. Scaiano, J. Pérez-Prieto, *J. Mater. Chem. B*, **2014**, 2, 4554-4563.
- 24 S. Lucky, N. Idris, Z. Li, K. Huang, K. Soo, Y. Zhang, *ACS Nano*, **2015**, 9, 191-205.
- 25 S. Cui, D. Yin, Y. Chen, Y. Di, H. Chen, Y. S. Achilefu, Y. Gu, *ACS Nano*, **2013**, 7, 676-688.
- 26 Z. Zhen, W. Tang, Y. Chuang, T. Todd, W. Zhang, X. Lin, G. Niu, G. Liu, L. Wang, Z. Pan, X. Chen, J. Xie, *ACS Nano*, **2014**, 8, 6004-6013.
- 27 L. Brannon-Peppas, J. O. Blanchette, *Adv. Drug Deliver. Rev.*, **2004**, 56, 1649-1659.
- 28 Q. Yuan, Y. Wu, J. Wang, D. Q. Lu, Z. L. Zhao, T. Liu, X. B. Zhang, W. H. Tan, *Angew. Chem. Int. Ed.*, **2013**, 52, 13965-13969.
- 29 Y. Choi, R. Weissleder, C. H. Tung, *Agent. Cancer Res.* **2006**, 66, 7225-7236.
- 30 K. Liu, X. Liu, Q. Zeng, Y. Zhang, L. Tu, T. Liu, X. Kong, Y. Wang, F. Cao, S. A. Lambrechts, *ACS Nano* **2012**, 6, 4054-4062.
- 31 A. Zhou, Y. Wei, B. Wu, Q. Chen, D. Xing, *Mol. Pharm.* **2012**, 9, 1580-1589.
- 32 D. M. Yang, P. A. Ma, Z. Y. Hou, Z. Y. Cheng, C. X. Li, J. Lin, *Chem. Soc. Rev.* **2015**, 44, 1416-1448.
- 33 V. Muhr, S. Wilhelm, T. Hirsch, O. S. Wolfbeis, *Acc. Chem. Res.* **2014**, 47, 3481-3493.
- 34 H. H. Gorris, O. S. Wolfbeis, Biomolecules, and Microspheres *Angew. Chem. Int. Ed.*, **2013**, 52, 3584-3600.

- 35 Z. J. Gu, L. Yan, G. Tian, S. J. Li, Z. F. Cai, Y. L. Zhao, *Adv. Mater.*, **2013**, 25, 3758-3779.
- 36 N. M. Idris, M. K. G. Jayakumar, A. Bansal, Y. Zhang, *Chem. Soc. Rev.* **2015**, 44, 1449-1478.
- 37 G. Obaid, I. Chambrier, M. J. Cook, D. A. Russell, *Angew. Chem. Int. Ed.*, **2012**, 51, 6158-6162.
- 38 H. Maeda, J. Wu, T. Sawa, Y. Matsumura, K. Hori, *J. Control. Release* **2000**, 65, 271-284.
- 39 K. Hayashi, M. Nakamura, H. Miki, S. Ozaki, M. Abe, T. Matsumoto, T. Kori, K. Ishimura, *Adv. Funct. Mater.*, **2014**, 24, 503-513.
- 40 C.-M. J. Hu, L. Zhang, S. Aryal, C. Cheung, R. H. Fang, L. F. Zhang, *Proc. Natl. Acad. Sci. USA*, **2011**, 108, 10980-10985.
- 41 C. Wang, X. Q. Sun, L. Cheng, S. N. Yin, G. B. Yang, Y. G. Li, Z. Liu, *Adv. Mater.* **2014**, 26, 4794-4802.
- 42 W. L. Ren, G. Tian, S. Jian, Z. J. Gu, L. J. Zhou, L. Yan, S. Jin, W. Y. Yin, Y. L. Zhao, *RSC Adv.* **2012**, 2, 7037-7041.
- 43 J. H. Shi, L. Kundrat, N. Pishesha, A. Bilate, C. Theile, T. Maruyama, S. K. Dougan, H. L. H. F. Ploegh, *Proc. Natl. Acad. Sci. USA*, **2014**, 111, 10131-10136.
- 44 X. H. Wang, H. S. Peng, L. Yang, F. T. You, F. Teng, L. L. Hou, O. S. Wolfbeis, *Angew. Chem. Int. Ed.*, 2014, 53, 12471-12475.
- 45 Q. L. Hu, M. Gao, G. X. Feng, B. Liu, *Angew. Chem. Int. Ed.* **2014**, 53, 14225-14229.
- 46 Z. G. Yang, J. H. Lee, H. M. Jeon, J. H. Han, N. Park, Y. X. He, H. Lee, K. S. Hong, C. Kang, J. S. Kim, *J. Am. Chem. Soc.*, **2013**, 135, 11657-11662.
- 47 C. Wang, L. Cheng, Z. Liu, *Theranostics*, **2013**, 3, 317-330.
- 48 M. Ethirajan, Y. H. Chen, P. Joshi, R. K. Pandey, *Chem. Soc. Rev.* **2011**, 40, 340-362.
- 49 Y. Yuan, J. Liu, B. Liu, *Angew. Chem. Int. Ed.*, **2014**, 53, 7163-7168.
- 50 P.-P. Lv, Y.-F. Ma, R. Yu, H. Yue, D.-Z. Ni, W. Wei, G.-H. Ma, *Mol. Pharm.*, **2012**, 9, 1736-1747.
- 51 R. H. Fang, C.-M. Hu, B. T. Luk, W. W. Gao, J. A. Copp, Y. Y. Tai, D. E. O'Connor, L. F. Zhang, *Nano Lett.* **2014**, 14, 2181-2188.
- 52 P. Costantini, E. Jacotot, D. Decaudin, G. Kroemer, *J. Natl. Cancer Inst.* **2000**, 92, 1042-1053.
- 53 S.-Y. Liu, W. Wei, H. Yue, D.-Z. Ni, Z.-G. Yue, S. Wang, Q. Fu, Y.-Q. Wang, G.-H. Ma, Z.-G. Su, *Biomaterials* **2013**, 34, 8291-8300.
- 54 S. R. Jean, D. V. Tulumello, S. P. Wisnovsky, E. K. Lei, M. P. Pereira, S. O. Kelley, *ACS Chem. Biol.*, **2014**, 9, 323-333.



A novel class of erythrocyte membrane (RM)-coated biomimetic nanovectors with programmed delivery and NIR light triggering properties is developed. The synergistic effect of superior stealth ability, high efficacy of $^1\text{O}_2$ generation and release that the RM coating enables, the tumor-targeting and mitochondria-guiding features of the agents is demonstrated and the improved photodynamic therapy efficacy in *in vivo* tumor-bearing mice is confirmed.